Journal of Environmental Management 405 (2026) 129639

Contents lists available at ScienceDirect

Journal of Environmental Management

journal homepage: www.elsevier.com/locate/jenvman

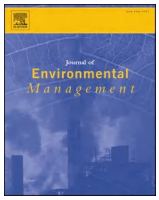

Research article

From degradation to conservation: Tracking mangrove dynamic changes of Hainan Island in China

Bingnan Zhao [a], Zhijun Dai [a,b,*], Yuan Xiong [a], Chuqi Long [c], Xuefei Mei [a], Jinping Cheng [c]

[a] State Key Laboratory of Estuarine and Coastal Research, East China Normal University, Shanghai, 200062, China
[b] Laboratory for Marine Geology, Qingdao Marine Science and Technology Center, Qingdao, China
[c] Department of Science and Environmental Studies, The Education University of Hong Kong, New Territories, Hong Kong, China

ARTICLE INFO

Keywords:
Mangrove forests
Gain and loss
Hainan island
Coastal dynamics
Ecological policies

ABSTRACT

Mangroves are vital coastal ecosystems in tropical and subtropical regions, providing critical services such as typhoon wave attenuation and carbon sequestration. However, these ecosystems face increasing natural and anthropogenic threats. Here, we analysed the spatiotemporal dynamics of mangroves within Hainan's protected areas using multi-temporal remote sensing data from 1988 to 2023 and the Random Forest (RF) classifier, dividing them into six study areas. Our results show a net mangrove loss of 129.25 ha, characterized by three distinct phases: degradation (1988–2003), stabilization (2003–2013), and slight expansion (2013–2023). Spatially, Dongzhaigang showed consistent growth, and Huachangwan recovered after early losses, while others experienced net losses. The spatial distribution of mangroves tends to expand seaward, while losses are predominantly concentrated in landward regions. Five of the six study areas are located within coastal lagoons, where sheltered conditions and sediment input driven by tidal currents and waves promote seaward mangrove expansion. Despite a relative sea-level rise of 4.44 mm/year, mangroves continued to expand seaward, demonstrating resilience against inundation pressures. These lagoons also provide ideal conditions for coastal aquaculture, particularly in the landward zones. Although these protected areas were primarily established in the 1980s, significant expanses of landward mangroves between 1988 and 2003 were transformed into aquaculture ponds. Following 2003, strengthened ecological policies successfully halted degradation, enabling widespread mangrove recovery. These findings provide critical insights for enhancing mangrove resilience and guiding global restoration initiatives.

1. Introduction

Mangrove forests are intertidal ecosystems that provide essential coastal protection, carbon sequestration, and fisheries support (Giri et al., 2011; Blanton et al., 2024). However, these critical ecosystems face dual pressures from human activities and climate change. Since the 1980s, aquaculture expansion, land reclamation, and coastal development have driven the loss of 20–35% of global mangrove forests (FAO, 2007, 2023). Meanwhile, rising sea levels are steadily eroding their habitat. When relative sea level rise exceeds 6–7 mm per year, most mangrove ecosystems struggle to maintain vertical growth and are at risk of inundation (Saintilan et al., 2020). If current trends continue, mangroves may largely disappear within this century (Sandilyan and Kathiresan, 2012). Therefore, the central scientific challenge is to understand how natural hydro-sedimentary processes and human interventions jointly shape mangrove expansion and loss. Understanding these mechanisms is essential for effective conservation and sustainable management of mangrove ecosystems.

Natural factors could substantially alter mangrove areas and distribution (Rakotomavo and Fromard, 2010; Le Nguyen and Luong, 2019). Sediment delivered by rivers to estuaries and broad deltas leads to deposition, which supports mangrove growth towards the sea (Wu et al., 2025). On tide-dominated coasts, tidal currents enhance sediment retention and promote seedling establishment, contributing to mangrove expansion (Amma and Bhaskaran, 2020; Jiang et al., 2025). Conversely, on wave-dominated coasts, sediment resuspension and erosion caused by wave energy restrict mangrove growth to sheltered zones behind sandbars or reefs (Long et al., 2025). Accelerated sea-level rise and extreme climatic events further threaten intertidal mangroves by overwhelming vertical accretion, resulting in prolonged flooding and

* Corresponding author. State Key Laboratory of Estuarine and Coastal Research, East China Normal University, Shanghai, 200062, China.
E-mail address: zjdai@sklec.ecnu.edu.cn (Z. Dai).

https://doi.org/10.1016/j.jenvman.2026.129639
Received 14 July 2025; Received in revised form 7 January 2026; Accepted 7 April 2026
Available online 13 April 2026
0301-4797/© 2026 Published by Elsevier Ltd.

elevated mortality (Taillie et al., 2020). To date, most studies have focused extensively on estuarine and deltaic regions (Adame et al., 2010; Dai et al., 2024), while the long-term dynamics and responses of mangroves in lagoon and reef environments remain relatively limited.

Anthropogenic disturbances, particularly aquaculture pond construction, are among the main causes of mangrove loss (Goldberg et al., 2020). Surveys from the 1980s–1990s found that over 50% of mangrove deforestation in major aquaculture-producing countries was directly linked to pond construction (Hamilton, 2013). Lagoon and reef environments are often considered highly suitable for aquaculture, yet the wealth of mangrove ecosystem services was little recognized during the early stages (Herbeck et al., 2020). As the importance of mangroves gained recognition over time, governments implemented conservation measures and established protected areas. When combined with strong governance, these measures have helped reduce mangrove loss and promote recovery (Nguyen et al., 2017; Gill et al., 2017). However, island lagoon and reef environments are complex socio-ecological systems, making it challenging to balance mangrove conservation with the economic benefits of aquaculture. The relative influence of governance and human activities on mangrove recovery remains unclear.

Mangroves inhabit low-energy intertidal zones where conducting conventional field surveys is logistically challenging and time-consuming (Bryan-Brown et al., 2020). Remote sensing provides a crucial tool for capturing both spatial and temporal changes in mangrove ecosystems, including their distribution, extent, and dynamics (Kuenzer et al., 2011; Giri, 2016). The use of long-term satellite time series, together with continuous land disturbance monitoring, enables the characterization of temporal continuity in mangrove change (Wang et al., 2019; Thomas et al., 2017). While coastal mangroves have been extensively studied, long-term dynamics of island mangroves remain poorly understood (Seto and Fragkias, 2007; Long et al., 2022). Recent advances in machine-learning techniques have further improved the accuracy and efficiency of mangrove mapping. Among these approaches, Random Forest is particularly effective due to its robustness to noise and its ability to capture complex, non-linear relationships (Belgiu and Drăguţ, 2016).

Hainan Island is a typical tropical Chinese island, boasting extensive lagoonal and reef-associated coastlines that provide sheltered environments ideal for mangrove development (Fu et al., 2024). Mangroves have been severely degraded by land reclamation and aquaculture expansion, but initiatives such as returning ponds to forests have promoted a gradual recovery (Zhu et al., 2021; Tian et al., 2024). Most studies focus on changes to mangrove areas and primarily attribute these changes to human activities (Zhang et al., 2021; Fu et al., 2022a). However, the roles of environmental dynamics, sedimentary processes, and geomorphological controls remain insufficiently explored (Bunting et al., 2022). Therefore, we used Landsat time-series imagery combined with a random forest model to map mangrove distribution and dynamics on Hainan Island from 1988 to 2023. Specifically, we aim to: 1) quantify spatiotemporal changes in mangrove extent within protected areas on Hainan Island; 2) discern the changes in mangrove shorelines; and 3) identify possible drivers influencing mangrove dynamics. The results advance understanding of long-term mangrove evolution on Hainan Island and offer implications for the sustainable management and conservation of lagoonal and island mangrove systems worldwide.

2. Materials and methods

2.1. Study area

Hainan Island, situated at the southernmost point in China (Fig. 1A), spans from 18°10′ N to 20°10′ N and 108°37′ E to 111°03′ E, covering an area of approximately 3.54×10^4 km^2. The island is located within the tropical monsoon climate zone, with an annual average temperature of

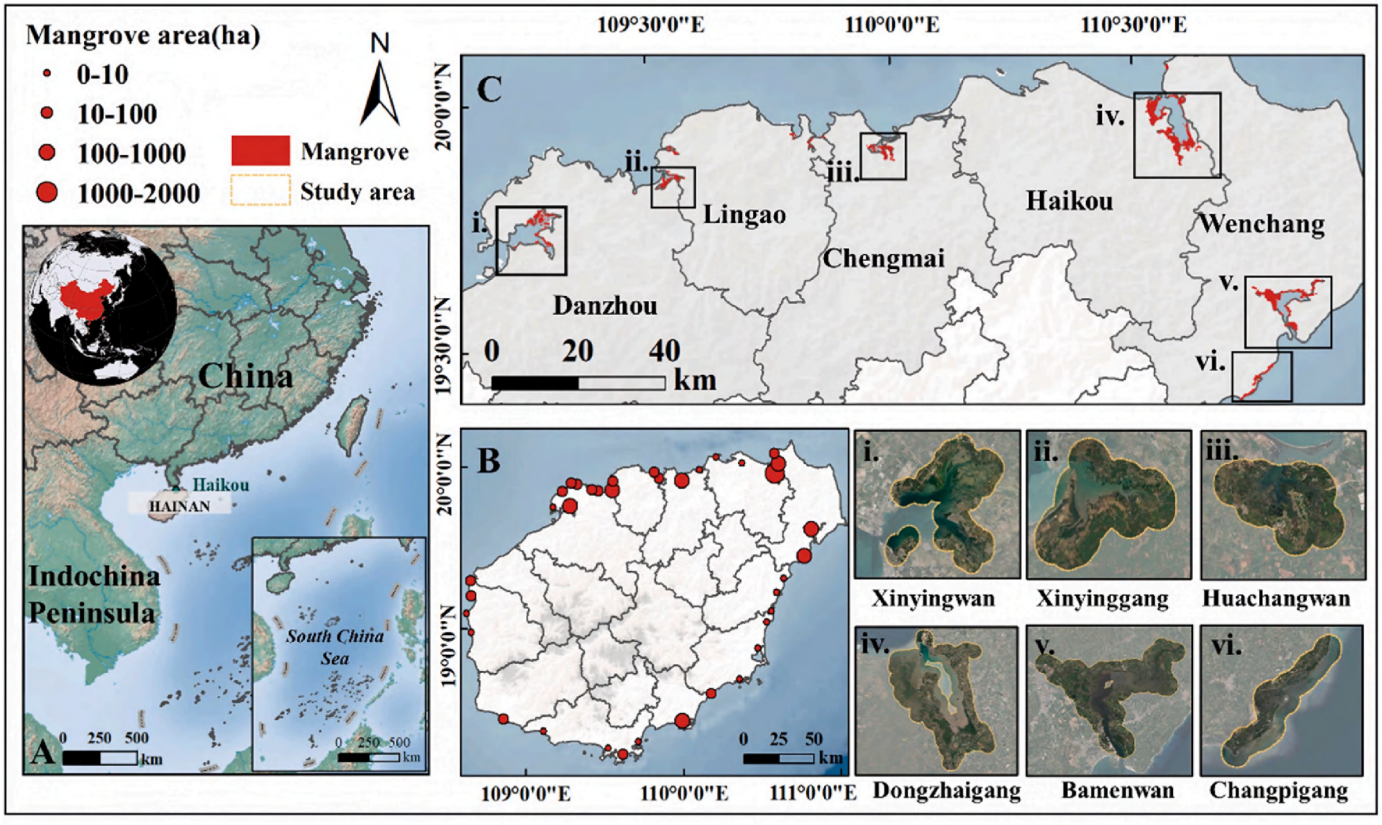

Fig. 1. Study area. (A) Location of the Hainan Island; (B) The distribution of mangroves in Hainan Island; (C)The Spatial distribution characteristics, and (i-vi) Specific morphology of the study area.

22.5–25.6 °C and abundant water and heat resources, providing favorable conditions for mangrove growth (Liu et al., 2007, 2022). The surrounding coastal waters are shaped by complex tidal regimes, including regular and irregular diurnal tides, with an average tidal range of 0.5–2 m throughout the year (Yuan et al., 2024). Furthermore, the monsoon system predominantly governs coastal wave direction, resulting in significant seasonal variability.

Hainan Island hosts one of China's most extensive and concentrated mangrove distributions, accounting for approximately 20–33% of the national total. Large, contiguous mangrove forests are primarily distributed in Dongzhaigang (Haikou), Bamenwan and Changpigang (Wenchang), Xinyingwan (Danzhou), and Xinyinggang (Danzhou–Lingao) (Fig. 1). Additional mangrove areas exist in Huachangwan of Chengmai County and in Changpigang of Wenchang. Even though smaller than the four major regions, they remain important components of Hainan's mangrove system. Smaller, more fragmented patches occur in locations such as the Sanya River estuary and Dongfang (Fig. 1B). According to the China Nature Reserve Directory, eight mangrove reserves have been designated on Hainan Island. Based on an integrated analysis of existing mangrove datasets, we selected six of these reserves as study sites. The excluded reserves were omitted primarily due to their small, fragmented patches, which present challenges for consistent, long-term classification using medium-resolution imagery. The selected reserves comprise one national (Dongzhaigang), one provincial (Qinglangang, including Bamenwan and Changpigang), and three county-level protected areas (Xinyingwan, Xinyinggang, and Huachangwan) (Table S1). Changpigang is located along a reef-fringed coastline, whereas the remaining sites are situated within lagoon systems. Collectively, these areas represent over 75% of Hainan's total mangrove extent, providing robust coverage for assessing island-scale mangrove dynamics (Meng et al., 2022; Li et al., 2022).

2.2. Materials

Landsat satellite imagery was used to analyze long-term mangrove area changes on Hainan Island. Images from Landsat 5 TM, Landsat 7 ETM+, Landsat 8 OLI, and Landsat 9 OLI-2 (Collection 2) covering 1988–2023 were obtained via Google Earth Engine (GEE) (https://earthengine.google.com). To ensure data quality, cloud-free or minimally cloudy scenes acquired under low-tide conditions were preferentially selected. All images were preprocessed using the World Geodetic System 1984 (WGS84) as the geographic coordinate system and WGS_1984_UTM_Zone_49N of the Universal Transverse Mercator (UTM) as the projected coordinate system. Cloud-covered pixels were processed using the Quality Assessment (QA) band in GEE, where clouds, cloud shadows, and aerosol-contaminated pixels were masked and replaced with cloud-free pixels from the same year. Mangrove extraction was not performed for 2012 due to insufficient image quality after cloud removal. Gaps caused by Landsat 7 scan line corrector (SLC) failure were filled using linear interpolation based on the same-year imagery. To maintain data quality and minimize potential SLC-related artifacts, images from other Landsat series were preferentially used whenever available.

Given that mangroves predominantly occupy low-lying intertidal zones, elevation data from the 30 m NASA SRTM Digital Elevation Model were included as an auxiliary classification band to improve mapping accuracy. Classification results were validated using reference samples from the Global Mangrove Watch (GMW) dataset (https://www.globalmangrovewatch.org/) and historical high-resolution imagery from Google Earth. To investigate the driving factors of mangrove area change, additional geophysical and oceanographic datasets were compiled. Wave direction and significant wave height (SWH) data spanning 1988–2023 were sourced from the European Centre for Medium-Range Weather Forecasts (ECMWF) (https://cds.climate.copernicus.eu/cdsapp#!/). Sea level data were obtained from the China Sea Level Bulletin (https://www.nmdis.org.cn/hygb/), and ocean current data were obtained from the Copernicus Marine Environment Monitoring Service (CMEMS) (https://data.marine.copernicus.eu/product/GLOBAL_MULTIYEAR_PHY_001_030). Sediment availability was assessed using MERIS-derived total suspended matter (TSM) data from the GlobColour project (http://globcolour.info), from which long-term mean TSM values were calculated to represent spatial patterns of sediment supply.

2.3. Methods

2.3.1. Data preparation

Regions of Interest (ROIs) were defined by generating 1 km buffers around the union of all pixels ever classified as mangrove in the GMW time series (Bunting et al., 2022). This buffer distance was chosen based on the typical width of mangrove patches on Hainan Island, ensuring inclusion of potential mangrove areas while minimizing interference from inland vegetation. Within each ROI, 250 mangrove and 250 non-mangrove sample points were automatically generated from areas consistently labeled as stable mangrove and stable non-mangrove throughout the GMW time series. All points were visually verified using high-resolution Google Earth. The 1 km buffer exceeds the typical width of mangrove stands, ensuring all relevant pixels are included, while the sample size provides sufficient spatial coverage to support a robust medium-resolution classification.

2.3.2. Calculation of vegetation indices

Mangroves exhibit distinct spectral characteristics relative to surrounding land-cover types (Zeng et al., 2022). To enhance classification accuracy, six vegetation indices were derived from the blue, green, red, near-infrared (NIR), and short-wave infrared (SWIR) bands. These indices include the Normalized Difference Vegetation Index (NDVI), Enhanced Vegetation Index (EVI), Land Surface Water Index (LSWI), Normalized Difference Mangrove Index (NDMI), Modified Normalized Difference Water Index (mNDWI), and Modular Mangrove Recognition Index (MMRI) (Table S2). NDVI and EVI characterize vegetation cover, soil, and water differences using the ratio between NIR and red bands (Rouse Jr et al., 1973; Huete et al., 2002). Compared to NDVI, EVI incorporates the blue band (BLUE) to correct for atmospheric and soil background effects, making it particularly effective for identifying dense mangrove canopies. LSWI, mNDWI and NDMI use differences in the spectral properties of moisture and water to distinguish mangroves from adjacent aquatic and terrestrial vegetation in areas affected by tides (Xiao et al., 2005; Xu, 2006; Shi et al., 2016). MMRI improves the ability to distinguish mangroves by taking into account differences in the spectral properties of vegetation, water and non-vegetated surfaces (Diniz et al., 2019). The combined use of these indices improves overall mangrove classification accuracy.

2.3.3. Random forest classification

The Random Forest (RF) algorithm (Breiman, 2001) is a supervised classification ensemble learning technique. It builds multiple decision trees and combines their predictions through majority voting to improve generalisation and classification accuracy. By integrating Bagging with random feature selection, RF reduces overfitting and is robust to high-dimensional data, noise, and outliers (Rodriguez-Galiano et al., 2012). Efficiently implemented on the GEE platform, RF can handle large-scale geospatial data and, when combined with vegetation indices and auxiliary features, accurately differentiates complex land cover types.

In this study, RF analysis was used to distinguish between mangrove and non-mangrove areas on Hainan Island, and to analyze their spatiotemporal changes. Six spectral vegetation indices and elevation data were selected as the input variables. The training and validation samples, as detailed in Section 2.3.1, were randomly divided, with 70% of the data points allocated to training and the remaining 30% to validation. The RF model was trained using parameter settings selected to

ensure robust and reliable classification (Table S3). This successfully captured the spatial distribution of mangroves across the study area. Subsequently, the classification results were visually refined using Google Earth, focusing only on narrow transitional zones or mangrove front edges where there were clear discrepancies from the initial classification. These adjustments were minor and did not affect the overall result. Finally, annual maps of mangrove forest changes from 1988 to 2023 were produced.

2.3.4. Extraction of mangrove forest shoreline

Investigating spatiotemporal patterns of mangrove gain and loss is essential for understanding degradation and restoration processes. Mangrove distribution maps from different periods were overlaid in ArcGIS to identify areas of mangrove gain and loss, with the Erase function used to delineate changes across successive time intervals. Mangrove shorelines are highly dynamic under combined natural and anthropogenic influences. In this study, mangrove shorelines were delineated in ArcGIS through manual digitization directly from the mangrove distribution maps generated in Section 2.3.2. The seaward boundary of mangrove patches was consistently identified and digitized as the shoreline. Shoreline data were extracted for eight periods (1988–2023) at five-year intervals and then smoothed using the Smooth Line tool in ArcGIS to remove minor geometric irregularities. Shoreline change was quantified using the Digital Shoreline Analysis System (DSAS), an ArcGIS extension developed by the USGS, which calculates shoreline change metrics such as the Linear Regression Rate (LRR) and Net Shoreline Movement (NSM) (Thieler et al., 2009). LRR, which estimates long-term shoreline change trends using least-squares regression, was adopted as the primary indicator of mangrove shoreline dynamics (Baig et al., 2020; Quang et al., 2021). Consequently, LRR was selected as the primary metric to assess mangrove shoreline changes on Hainan Island. In total, 2057 transects were generated to quantify

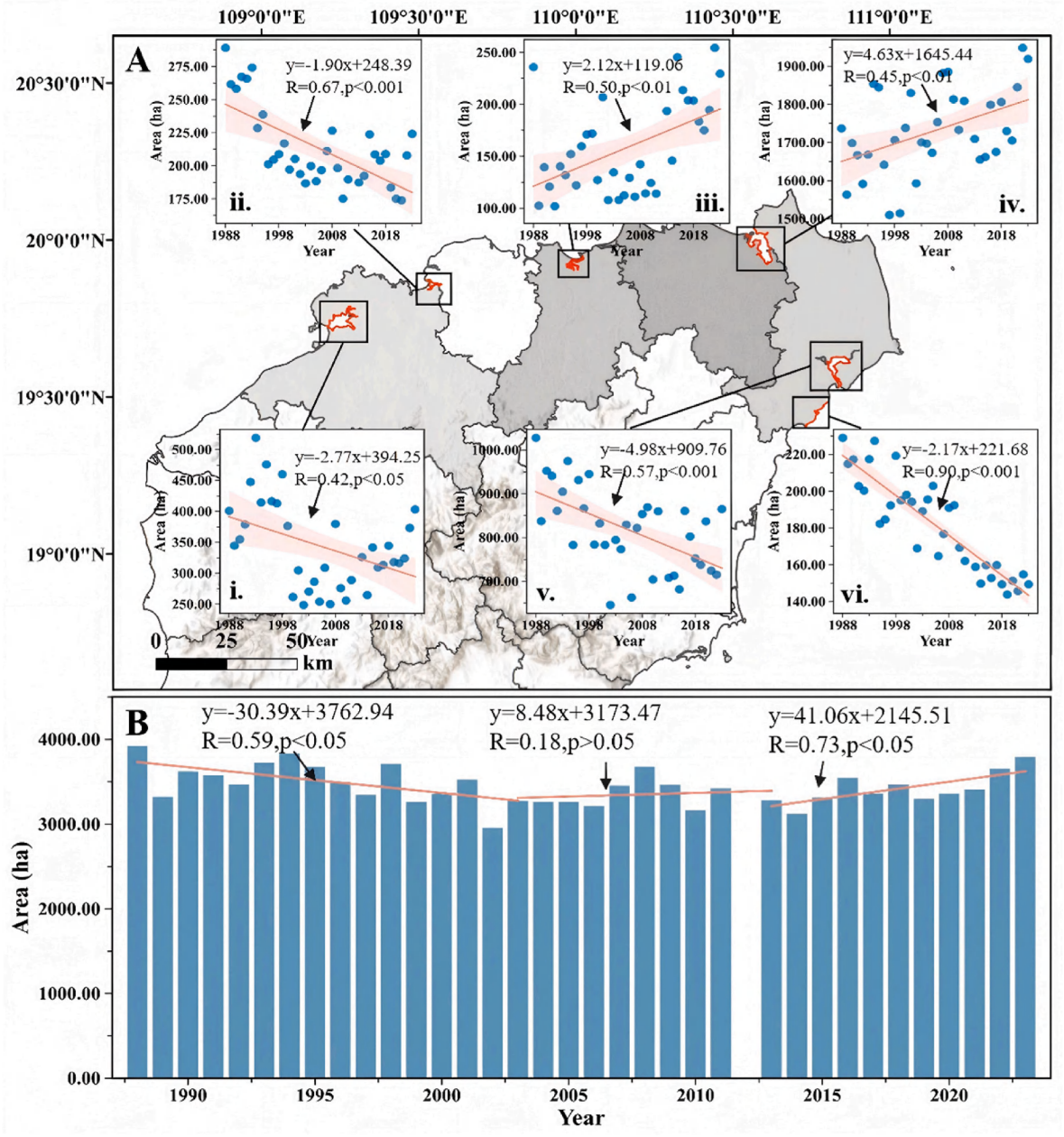

Fig. 2. Temporal variation of mangrove forest area in Hainan Island. A: The temporal variation in the area of mangroves by region; B: Time variation of the total mangrove forest area.

shoreline changes from 1988 to 2023. To assess the capacity of mangrove forests to sustain seaward expansion under sea-level rise, the average vertical sediment accumulation rate (AVSA) was calculated following (Xiong et al., 2024; Wu et al., 2025):

$$AVSA = V\tan\theta \quad (1)$$

where V is the average accretion rate of shorelines, and θ is the average slope across the six study areas obtained from the DEM.

2.3.5. Accuracy assessment

The classification accuracy was evaluated using a combination of high-resolution Google Earth. Overall Accuracy and the Kappa coefficient were calculated from the independent validation samples described in Section 2.3.1 using the confusion matrix. The Random Forest model consistently achieved an Overall Accuracy above 0.93 and a Kappa coefficient greater than 0.87 (Table S4), demonstrating reliable discrimination between mangrove and non-mangrove classes. In addition, shoreline change analysis using DSAS incorporated a 95% confidence interval to estimate the associated uncertainty. This approach further enhanced the robustness of the estimated shoreline trends (Nassar et al., 2019).

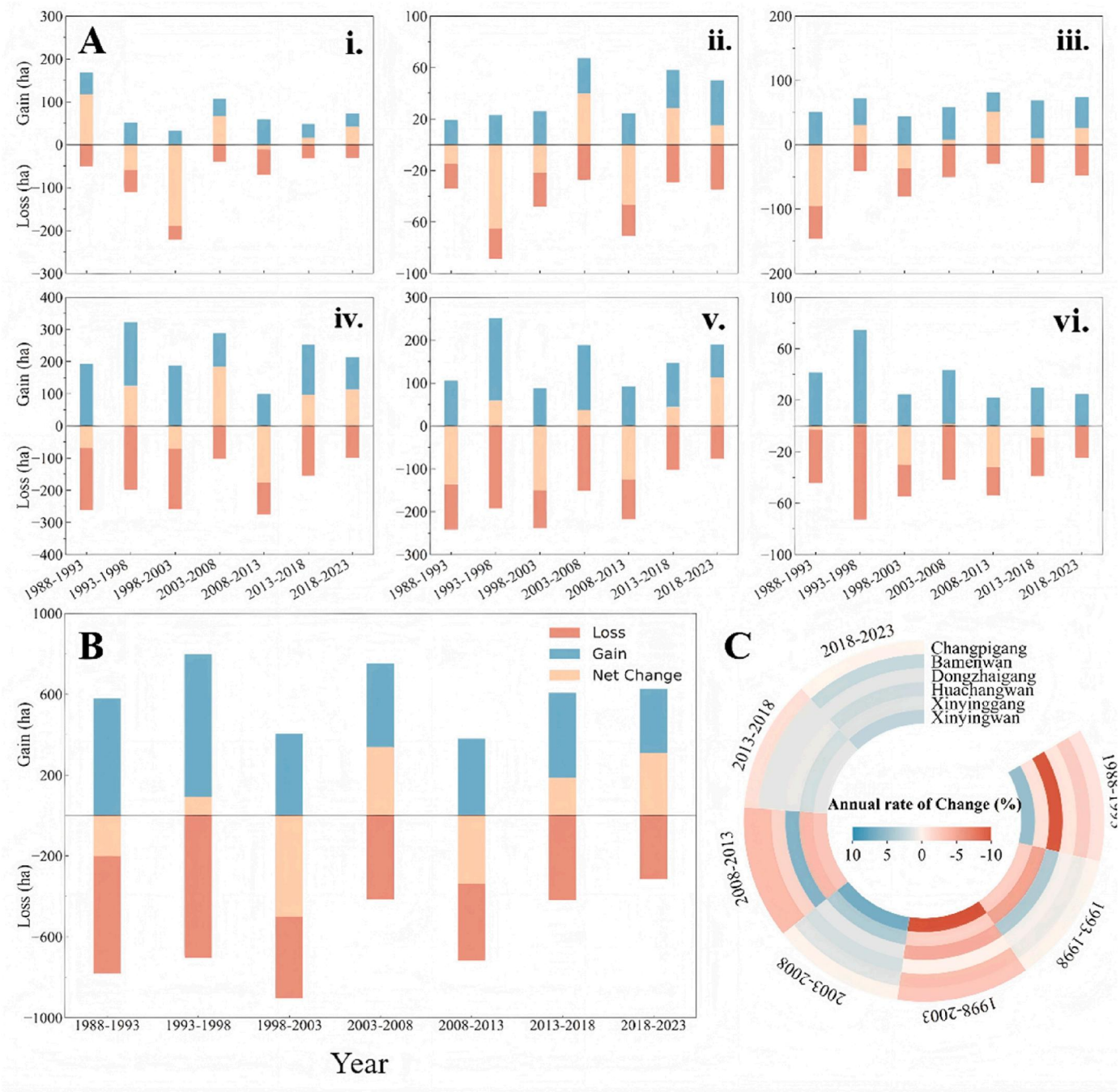

Fig. 3. Losses and gains of mangrove forest every 5 years in Hainan Island. A: Mangrove forest losses and gains in six study areas.; B: Total losses and gains of mangrove forest across the study area; C: Annual rate of change (%) in the area of mangrove forests.

3. Results

3.1. Variations in mangrove forest area

The area of mangroves from 1988 to 2023 showed a declining trend, ranging from 3920.50 ha to 3791.25 ha, with a decrease of 3.30%. Despite this net loss, mangrove dynamics exhibited pronounced temporal variability and can be divided into three distinct phases: rapid decline (1988–2003), relative stability (2003–2013), and gradual expansion (2013–2023) (Fig. 2B). During the rapid decline phase (1988–2003), mangrove area decreased markedly by 644.34 ha, from 3920.50 ha to 3276.16 ha, at an average rate of 30.39 ha/yr. This was followed by a period of relative stability between 2003 and 2013. During this time, the area of mangroves fluctuated, resulting in a negligible net change of 7.67 ha, equivalent to an annual change rate of just 0.023%. In contrast, the most recent phase (2013–2023) was characterized by sustained recovery, with mangrove area increasing by 507.42 ha at an average rate of 41.06 ha/yr (Fig. 2B).

In Dongzhaigang, the mangrove area increased from 1737.19 ha in 1988 to 1919.11 ha in 2023, with an average annual growth of 4.63 ha/yr (Fig. 2A(iv)). Similarly, Huachangwan exhibited a net increase of 2.12 ha yr^{-1} (Fig. 2A(iii)), despite a localized decline of 36.53 ha during 1998–2003 (Fig. 3A(iii)). This decline was followed by a period of stabilization and subsequent gradual recovery. In contrast, other regions experienced varying degrees of mangrove loss over the study period. Changpigang and Bamenwan experienced substantial long-term losses, with mangrove areas decreasing by 34.77% and 15.82%, respectively, between 1988 and 2023 (Fig. 2A(v-vi)). Xinyingwan and Xinyinggang also showed overall declining trends, particularly during 1993–2003, when mangrove area decreased by 47.87% and 31.93%, respectively. Both regions exhibited signs of gradual recovery after 2013 (Fig. 2 A(i-ii)).

3.2. Gain and loss in mangrove forest area

From 1988 to 2023, mangrove forests on Hainan Island exhibited an overall trajectory of initial loss followed by subsequent recovery, with pronounced non-linear interannual variability (Fig. 3C). Between 1988 and 2003, mangrove area declined markedly, with losses predominantly concentrated on the landward side (Fig. 4). From 1988 to 1993, a net loss of 200.59 ha was recorded (Fig. 3C; Fig. 4). Except for Xinyingwan, all other sites experienced varying mangrove loss (Fig. 3A(i); Fig. 4i).

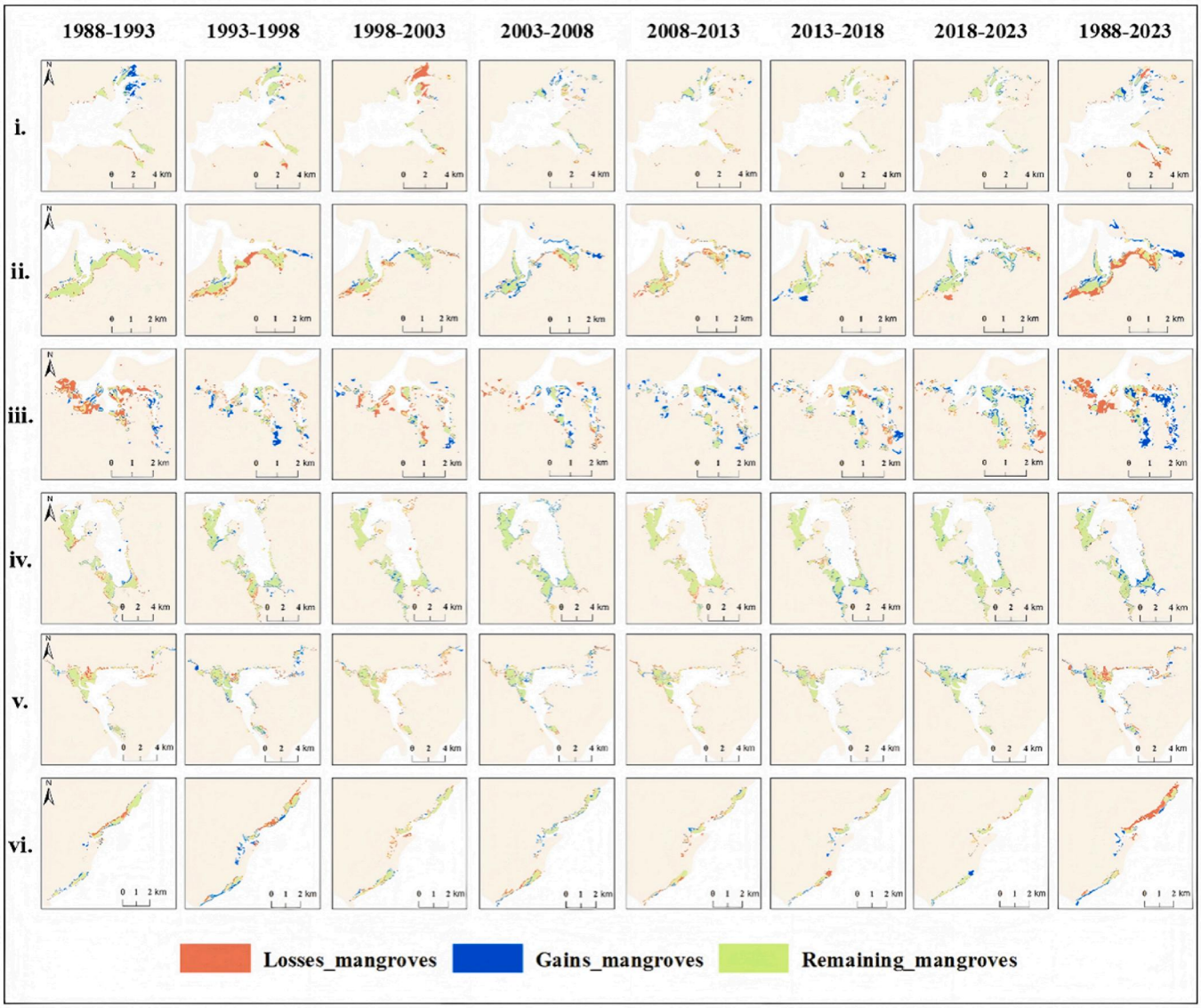

Fig. 4. Spatial distribution of losses and gains of mangrove forests within the Hainan Island from 1988 to 2023.

Significant net losses of mangrove forests were observed in Bamenwan and Huachangwan, with respective reductions of 136.14 ha and 95.60 ha (Fig. 3A(iii,v)). Although Dongzhaigang experienced the largest gross loss, mainly along the landward boundary, this was largely offset by seaward expansion, resulting in a relatively small net loss of 69.12 ha (Fig. 3A(iv); Fig. 4 iv). From 1993 to 1998, mangrove loss was concentrated in Xinyingwan and Xinyinggang, with net losses of 58.96 ha and 65.47 ha, respectively (Fig. 3 A(i-ii)). In particular, further degradation was recorded in the southern part of Xinyingwan, while a significant inland-to-seaward area was lost in the central region of Xinyinggang. From 1998 to 2003, all six study areas experienced mangrove loss with a total net loss of 500.79 ha (Fig. 3). Xinyingwan was most severely affected, losing 221.93 ha, primarily due to extensive inland erosion in its northern sector (Fig. 4).

Between 2003 and 2013, mangrove forest loss significantly declined, and the area entered a gradual recovery phase. From 2003 to 2008, significant restoration occurred in Dongzhaigang and Xinyingwan, where 288.11 ha and 106.75 ha of mangroves were gained, respectively (Fig. 3A). The areas of mangrove gain were primarily concentrated in regions that had experienced loss between 1988 and 2003, as well as on the seaward side (Fig. 4). Additional expansion was also observed in Bamenwan, Changpigang, Huachangwan, and the eastern portions of Xinyinggang. However, during 2008–2013, expansion slowed and renewed landward losses occurred in Bamenwan, Dongzhaigang, and Xinyinggang (Fig. 4), indicating continued spatial heterogeneity and ecological instability.

Between 2013–2018 and 2018–2023, mangrove forests in the study area exhibited a sustained recovery trend, with a total increase of 495.07 ha. Dongzhaigang experienced the largest increase in mangrove area, with gains of 252.31 ha and 212.85 ha, respectively (Fig. 3 A(iv)). After 2018, Bamenwan's mangrove area also grew significantly, showing a net increase of 113.02 ha (Fig. 3A (v)). Meanwhile, increases in coverage were observed in Huachangwan, the northern part of Xinyingwan, and the southern part of Changpigang (Fig. 4). Overall, mangrove loss between 1988 and 2023 was predominantly concentrated on the landward side. However, mangrove expansion was primarily observed in two distinct areas: the first being seaward expansion near the seaward, and the second being restoration within areas that had

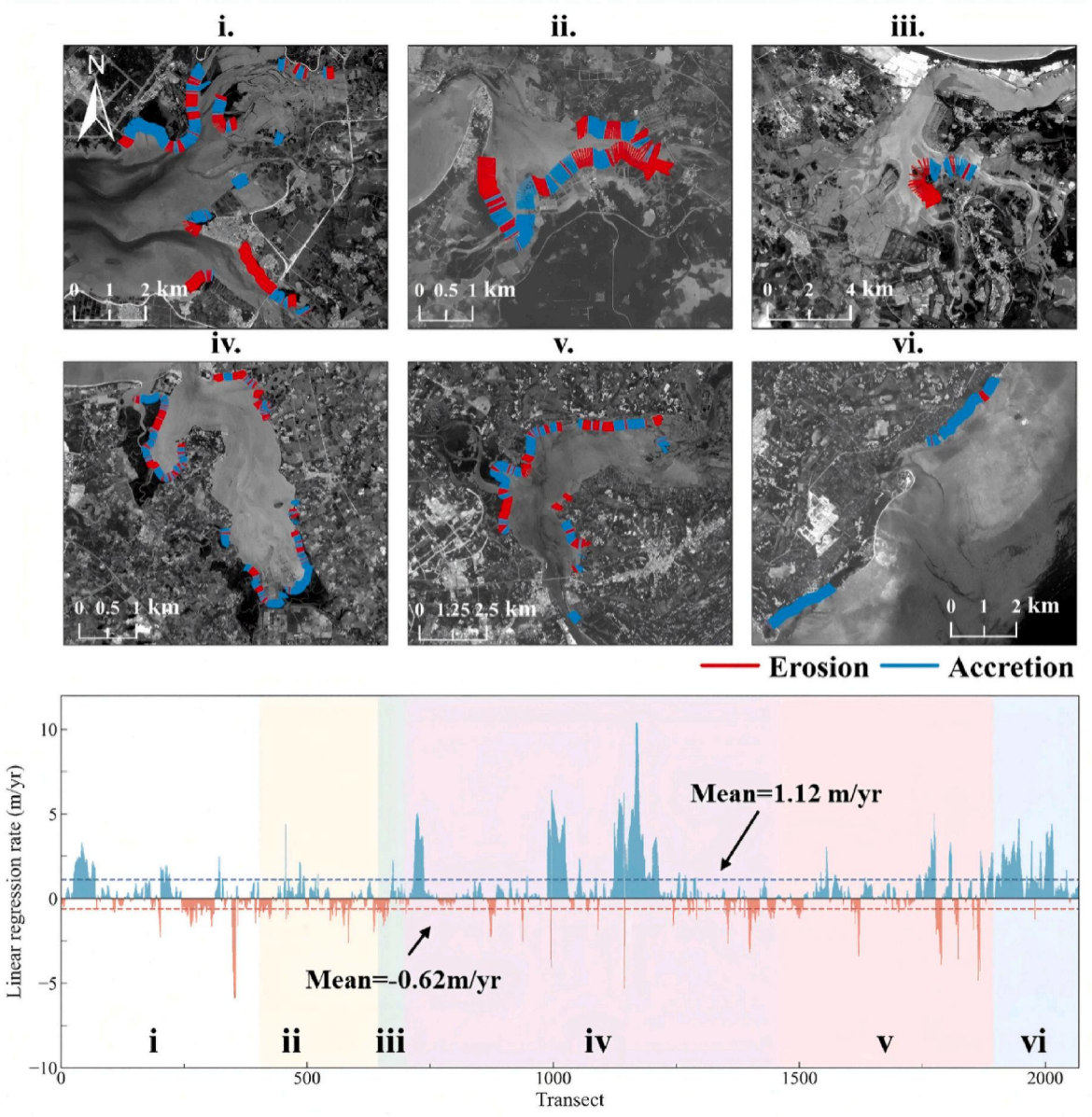

Fig. 5. Quantitative analysis of shoreline gains and losses of Hainan Island from 1988 to 2023.

previously experienced mangrove loss (Fig. 4). Notably, the mangrove patches in Dongzhaigang are more intact, with no significant losses observed in most areas (Fig. 4iv). Although restoration by 2023 did not fully offset the 36-year losses, recent trends indicate a consistent and steady expansion of mangrove coverage.

3.3. Mangrove forests shoreline changes

Over the past several decades, the mangrove forests along Hainan Island have exhibited a notable trend of seaward expansion (Fig. 5). From 1988 to 2023, the annual average change rate of the mangrove shorelines was 0.40 ± 0.33 m/yr. Among the observed sections, 786 erosion segments accounted for 37.97% of the total, with an average erosion rate of 0.62 m/yr. In contrast, 1284 gain segments comprised 62.03% of the total, with an average gain rate of 1.12 m/yr, indicating a general tendency for mangroves to advance seaward in most areas (Fig. 5; Table S5).

It is worth noting that the change varies significantly across different regions. Among the regions studied, Changpigang exhibits the highest seaward migration rate, with an annual average of 1.43 ± 0.32 m/yr. Approximately 57.14% showed significant expansion, reflecting the rapid growth trend of mangroves in this area (Fig. 5vi; Table S5). Dongzhaigang showed the second-highest change, with an average rate of 0.72 ± 0.3 m/yr, particularly in the southeast and southwest, where some areas experienced expansion rates exceeding 10 m/yr (Fig. 5iv; Table S5). Moreover, shoreline changes in Xinyingwan and Bamenwan exhibited relatively minor but consistent seaward advances at low rates, with more notable expansion occurring at river outlets (Fig. 5i,v). Shoreline changes in Xinyinggang and Huachangwan were minimal, characterized by alternating erosion and accretion, indicating a relatively stable mangrove boundary throughout the study period (Fig. 5ii-iii). Importantly, Dongzhaigang experienced a total mangrove loss of 222.34 ha. Seaward expansion accounted for roughly 146.46 ha, offsetting about 66% of the loss. This underscores the vital role of seaward growth in mitigating inland mangrove degradation.

4. Discussion

4.1. Impacts of ocean dynamics

Mangrove shorelines on Hainan Island display a coherent spatial pattern, with seaward expansion consistently linked to wave attenuation

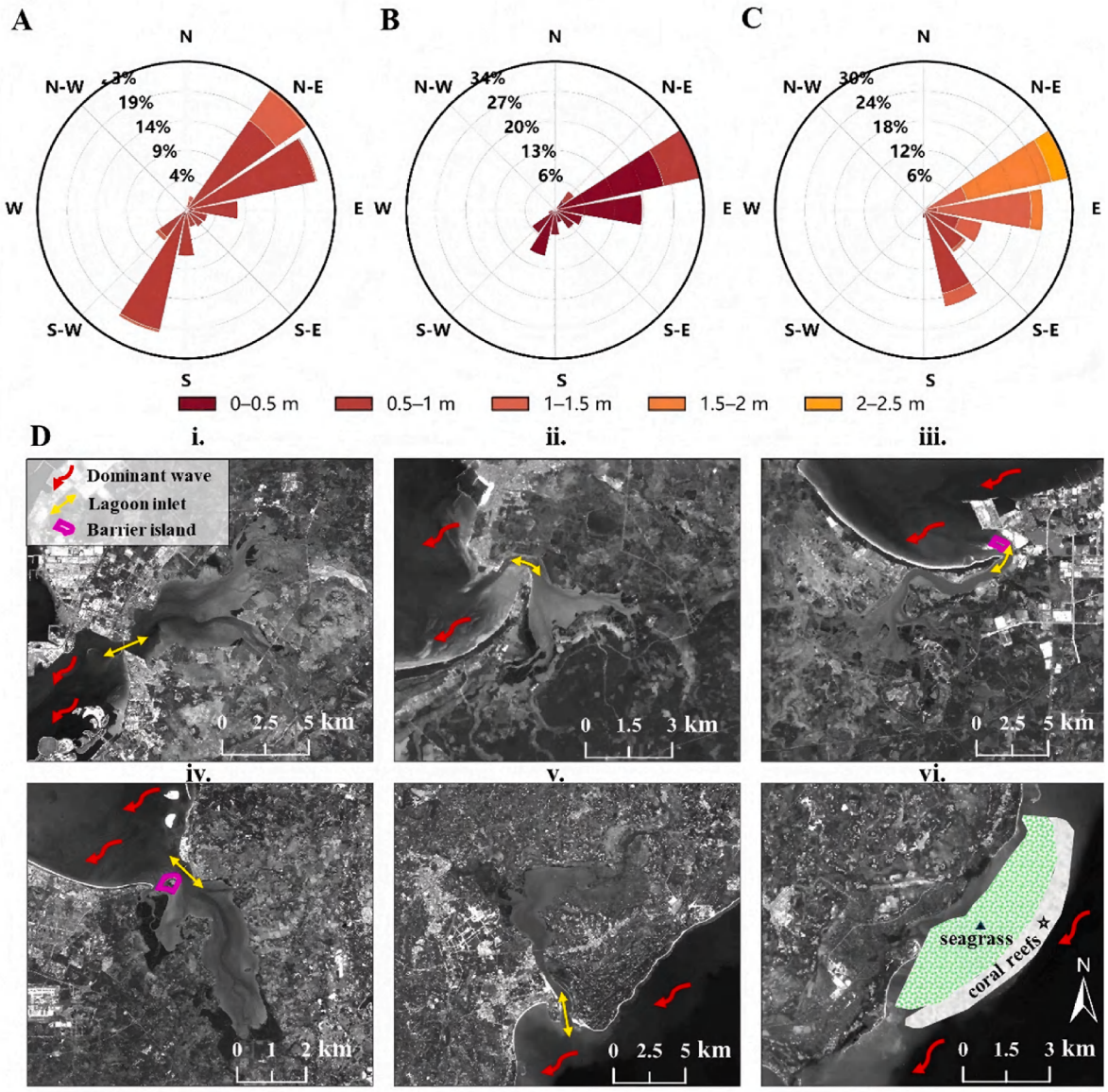

Fig. 6. Wave characteristics in different regions of Hainan Island. (A) Northwest Part. (B) North Part. (C) Northeast Part. (D) Dominant wave propagation pathways.

and sufficient sediment supply provided by fringing coral reefs and semi-enclosed lagoon systems. These settings generate persistently low-energy, sediment-favorable conditions, as dominant wave and tidal current directions remain broadly stable through time (Fig. S1; Fig. S2). In contrast, sites with restricted tidal exchange and limited sediment supply exhibit near-equilibrium or weak expansion, highlighting the combined control of ocean dynamics and geomorphic configuration.

4.1.1. Wave action

Wave conditions regulate mangrove persistence and seaward expansion by controlling nearshore hydrodynamic energy and sediment stability (Stone et al., 2005; Long et al., 2025). Analysis of shoreline and mangrove extent changes between 1988 and 2023 indicates that, on Hainan Island, mangrove shorelines have generally been in a state of seaward expansion. Two geomorphic features largely support this expansion: direct protection by fringing coral reefs and enclosure within semi-enclosed lagoon systems bounded by Sandbars. Wave-direction diagrams reveal pronounced spatial heterogeneity along the northwest (NW), north (N), and northeast (NE) coasts of Hainan Island (Fig. 6).

Along the NE coast at Changpigang, mangroves are directly exposed to offshore waves, with a mean significant wave height of approximately 1.22 m and more than 60% of wave events exceeding 1 m (Fig. 6C). Such energetic conditions would normally inhibit mangrove persistence through wave-driven erosion. However, observations indicate that mangrove fronts expanded seaward at a mean rate of 1.43 ± 0.32 m/yr (Fig. 5). This expansion is attributed to the extensive fringing coral reefs and seagrass meadows at the mangrove front, which act as an effective biogeomorphic buffer (Fig. 6D). By dissipating wave energy through friction and wave breaking, these structures reduce erosive stress at the mangrove fringe (Fu et al., 2022b; Harris et al., 2018).

In the other five study areas, mangroves are embedded within semi-enclosed lagoon systems. These lagoons are commonly surrounded by sandbars or barrier islands that intercept incoming waves and reduce the wave energy reaching the mangrove edge. Offshore wave climates vary from moderate conditions along the northwest coast to higher-energy regimes along the northeast coast (Fig. 6A–C), yet the interior lagoon environments remain consistently sheltered. Along the northwest coast, wave directions alternate between northeast (NE) and southwest (SW), with an average significant wave height of ~0.75 m and small waves (H < 1.0 m) accounting for nearly 90% of events (Fig. 6A). In the N and NE zones, waves travelling from the NE predominate. Geomorphic features such as deep channels in the N region reduce wave energy to an average of ~0.38 m (Fig. 6B; Zhou et al., 2024). For instance, at Huachangwan and Dongzhaigang on the N coast, a prominent barrier island intercepts waves from the dominant NE direction, creating a low-energy leeward environment (Fig. 6D). Similar wave-buffering effects operate across other lagoonal mangrove systems, limiting direct wave penetration and suppressing shoreline erosion (Fig. 6D).

4.1.2. Tidal current modulation of sediment dynamics

While wave attenuation stabilizes shoreline conditions, tidal currents are the main mechanism driving sediment transport and retention, which directly control seaward mangrove expansion (Fenies and Faugères, 1998). As depicted in multi-year average sea surface current maps from 1993 to 2023 (Fig. 7; Fig. S2), tidal currents promote sediment deposition and mitigate upstream sediment deficiencies.

Sites with narrow tidal inlets experience limited sediment delivery and retention by tidal currents, restricting mangrove accretion. Along the N coast, including Xinyinggang and Huachangwan, weak tidal forcing and restricted riverine inputs limit sediment supply to intertidal zones. Tidal currents are predominantly alongshore, favoring E–W sediment transport and deposition on sandbanks and barrier islands rather than within mangrove fronts (Fig. 7). As a result, sediment accumulation within intertidal areas remains insufficient to support lateral mangrove expansion, leading to near-equilibrium shorelines at these sites (Fig. 5). Despite having similarly constrained tidal currents due to its narrow and meandering inlets, Bamenwan receives a substantial amount of fluvial sediment input (1.0×10^5 t/yr) from the Wenjiao and Wenchang rivers (Xin et al., 2013), which supports moderate seaward expansion (Fig. 5).

In lagoon systems where tidal currents and riverine inputs jointly supply sediments, mangrove expansion is more evident. At Xinyingwan, sediment inputs from the Beimen and Chunjiang rivers provide the primary material for progradation (Gan et al., 2018). Seasonal variability in tidal currents modulates sediment retention: summer inflow enhances sediment import and deposition within the lagoon, whereas winter ebb-dominated flows promote sediment export, limiting net accretion (Fig. 7; Fig. S3). Consequently, mangrove expansion remains modest, averaging 0.16 m/yr. Dongzhaigang represents an efficient depositional system, where E–W tidal currents transport resuspended marine sediments into the lagoon (Fig. 5), while multiple rivers provide sustained fluvial inputs (Li et al., 2017). These combined sources form extensive intertidal mudflats that facilitate consistent mangrove establishment, supporting seaward expansion at an average rate of 0.72 ± 0.3 m/yr, with localized rates exceeding 5 m/yr (Fig. S3; Fig. 5).

At Changpigang, mangroves occur in an open coastal setting but experience strong hydrodynamic attenuation from extensive fringing coral reefs and seagrass meadows (Fig. S3). Predominantly alongshore tidal currents transport sediments that settle over these biogeomorphic features, enhancing sediment trapping at the mangrove front and producing the highest observed seaward expansion rate (Fig. 7; Table S5).

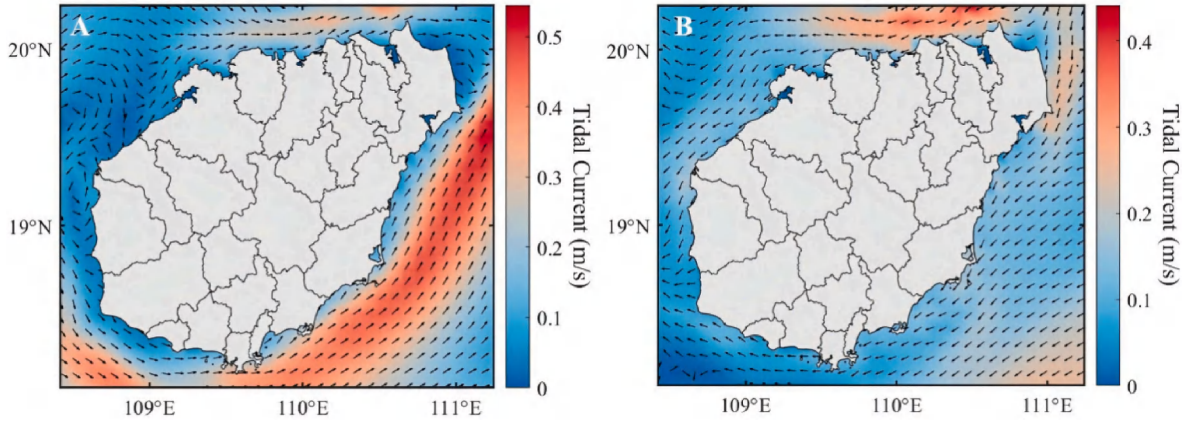

Fig. 7. Seasonal variation in tidal current along Hainan Island. (A) Summer. (B) Winter.

4.2. Sea level rise

Sea level rise (SLR) is commonly associated with landward mangrove migration under increased inundation stress (Di Nitto et al., 2014; Nevermann et al., 2023). Sea level data from Haikou Station (1980–2023) show a significant rise at a mean rate of 4.44 mm/yr (Fig. 8). Despite this rise, mangroves across the study area expanded seaward at an average rate of approximately 0.40 m/yr from 1988 to 2023 (Fig. 5). The AVSA, as calculated using Eq. (1), was found to be 58.16 mm/yr. This figure substantially exceeds the regional SLR rate and indicates that vertical accretion is currently offsetting inundation stress. This reflects a positive biogeomorphic feedback in which sufficient sediment supply and mangrove retention jointly sustain accretion and promote further expansion (Xie et al., 2022). Consequently, present SLR rates do not pose an immediate threat of widespread mangrove submergence on Hainan Island. However, this response is conditional rather than universal. Sediment-limited or near-equilibrium systems, such as Xinyinggang and Huachangwan, may be unable to maintain elevation relative to accelerating SLR or declining sediment supply. In such systems, a shift from seaward expansion to shoreline retreat is more likely under future climate scenarios. Overall, mangrove responses to SLR are governed less by the absolute rate of sea-level rise than by the balance between local sediment accumulation capacity and inundation pressure.

4.3. Destruction from human activities

Mangrove ecosystems on Hainan Island have experienced substantial anthropogenic pressure, primarily driven by aquaculture expansion since the 1990s (Yu et al., 2023; Herbeck et al., 2020). Economic reforms in Hainan Province aimed at promoting aquaculture have facilitated the expansion of fish farming, resulting in large-scale reclamation of coastal wetlands and mangrove areas for aquaculture ponds (Herbeck et al., 2013). In the study area, mangrove loss closely mirrored the spatial and temporal expansion of aquaculture ponds (Fig. 3). To illustrate the spatial impacts of pond encroachment, Fig. 9 shows transformations in four severely degraded regions. Aquaculture ponds initially concentrated along inland boundaries and progressively encroached into core forest areas. After 2013, mangrove cover increased as pond expansion slowed and abandoned or converted ponds facilitated recovery, as evidenced by 2023 satellite imagery (Fig. 9A–C, D). However, remaining ponds along forest margins continue to constrain mangrove expansion. Consistent with this pattern, current aquaculture pond distribution is negatively correlated with mangrove cover (Fig. S4; Zhang et al., 2022). Rapid pond growth between 1988 and 2003 coincided with peak mangrove loss at an average rate of 86.03 ha/yr. This rate declined to 59.48 ha/yr between 2003 and 2013 and further to 33.29 ha/yr by 2023, reflecting slowed pond expansion and increased abandonment or conversion of ponds, which facilitated partial mangrove recovery.

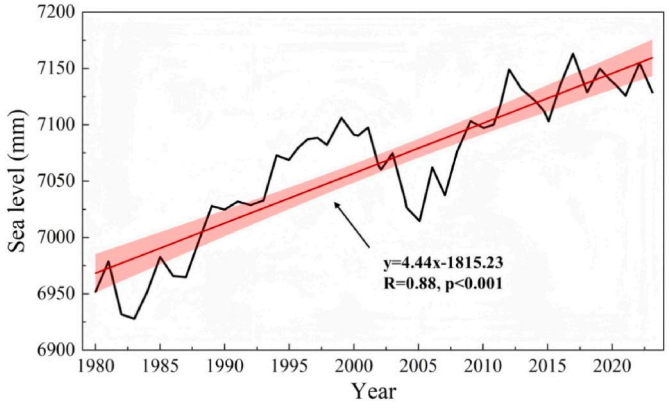

Fig. 8. The sea level rise and its simple linear regression analysis from 1980 to 2023.

Aquaculture infrastructure has also altered local hydrodynamics and sedimentary environments. For instance, in the vicinity of Changpigang, pond embankments, drainage channels, and intake pipes disrupt tidal exchange, modify sediment transport pathways, and hinder mangrove seedling establishment (Fig. S5A). Moreover, the extensive passage of these pipes through core conservation zones has not only disrupted the integrity of mangrove habitats but also caused water pollution (Fig. S5B). This indicates that aquaculture, while boosting economic development, directly threatens mangroves.

4.4. Policy implications and strategies for sustainable mangrove management

Policy interventions have played a central role in shaping mangrove dynamics on Hainan Island. Island-wide trends in mangrove area reflect three distinct phases: ineffective early protection before 2003, stabilization under improved regulation between 2003 and 2013, and active restoration after 2013 (Fig. 10A). During the initial phase, weak enforcement led to a cumulative loss of approximately 644.34 ha of mangroves. Subsequent implementation of targeted protection plans curtailed large-scale deforestation, while post-2013 restoration initiatives emphasized pond-to-wetland conversion, artificial planting, and ecological rehabilitation. Under the 13th Five-Year Plan, approximately 2933 ha of aquaculture ponds were converted into wetlands, and over 800 ha of mangroves were newly planted, representing an integrated restoration model combining pond-to-wetland conversion, artificial planting, and ecological rehabilitation.

Despite overall recovery, mangrove responses exhibit pronounced spatial heterogeneity, reflecting interactions among sediment availability, historical disturbance, and management intensity (Fig. 10B), which classifies systems into four types based on sediment and progradation potential and human pressure. Sediment-rich, well-protected systems such as Dongzhaigang achieved continuous natural expansion due to intact sediment connectivity and early legal designation. By contrast, historically degraded or sediment-limited sites, such as Huachangwan, required sustained government-led restoration to approach pre-disturbance coverage, whereas other reserves with weak enforcement continued to lose area. These patterns indicate that policy effectiveness is contingent on both environmental capacity and management, highlighting that early protection is more cost-effective than post hoc restoration and that legal designation alone is insufficient. Site-specific strategies are therefore essential to match local sedimentary and disturbance conditions.

In sediment-rich systems, natural sediment accretion and seedling establishment drive sustained expansion (Fig. 10B), whereas regions with limited sediment or altered hydrodynamics rely on continuous planting and engineering maintenance (Fig. S6). Notably, unchecked expansion in sediment-rich lagoons may reduce open-water areas through sediment infilling, emphasizing the need to balance afforestation with habitat heterogeneity. From a management perspective, effective mangrove conservation integrates island-scale patterns with local mechanisms, connecting policy actions to ecological outcomes. Recommended strategies include: (1) strict protection of core forests; (2) targeted pond-to-mangrove conversion in sediment-limited areas; and (3) restoration of sediment pathways and migration corridors guided by local sedimentation rates, supporting near-natural recovery while maintaining habitat heterogeneity.

4.5. Uncertainty analysis

This study employed the RF method combined with remote sensing imagery to select six mangrove nature reserves on Hainan Island, focusing on analyzing the spatiotemporal dynamics of their mangrove areas. While the classification is generally reliable, several uncertainties

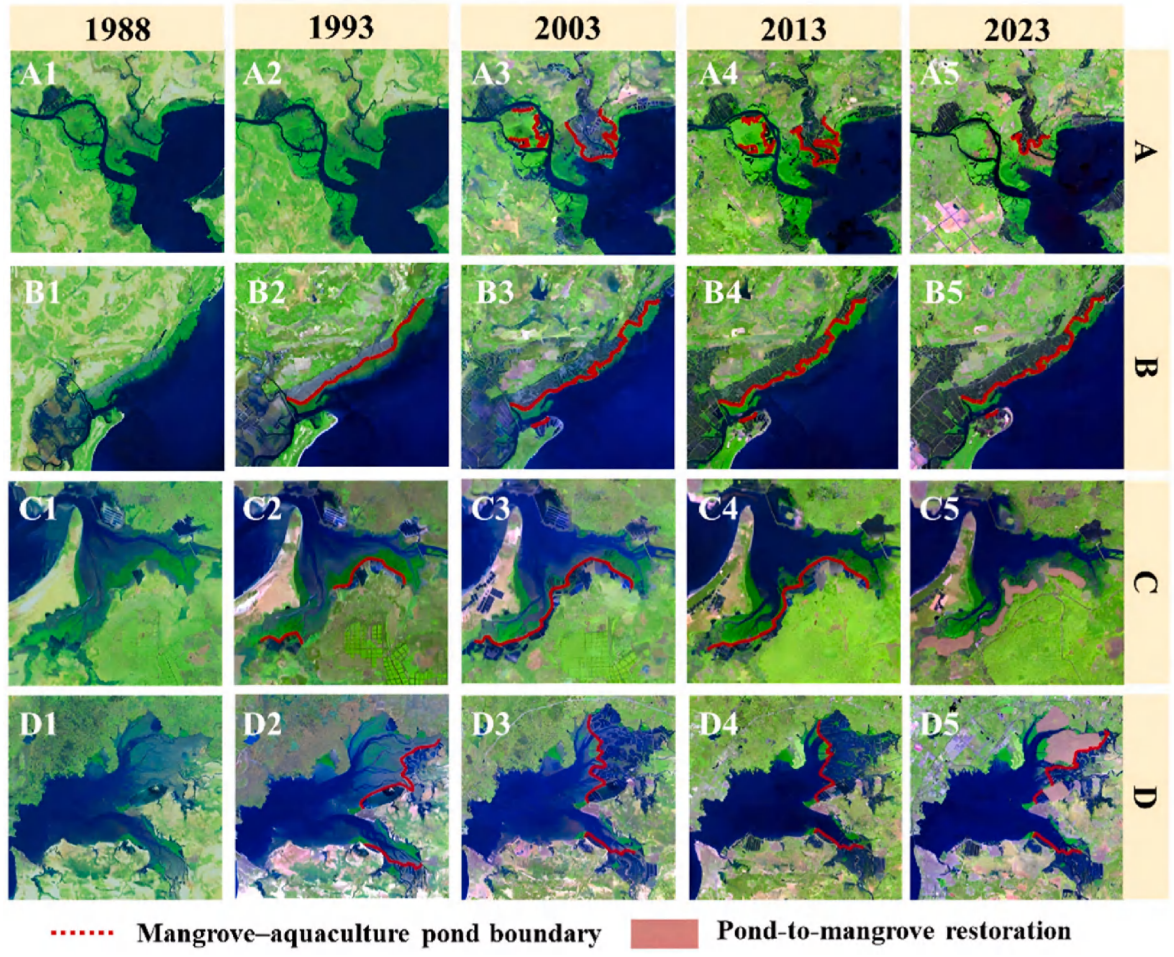

Fig. 9. Aquaculture pond encroachment on mangroves in typical areas of hainan island. (A) Bamenwan. (B) Changpigang. (C) Xinyinggang. (D) Xinyingwan.

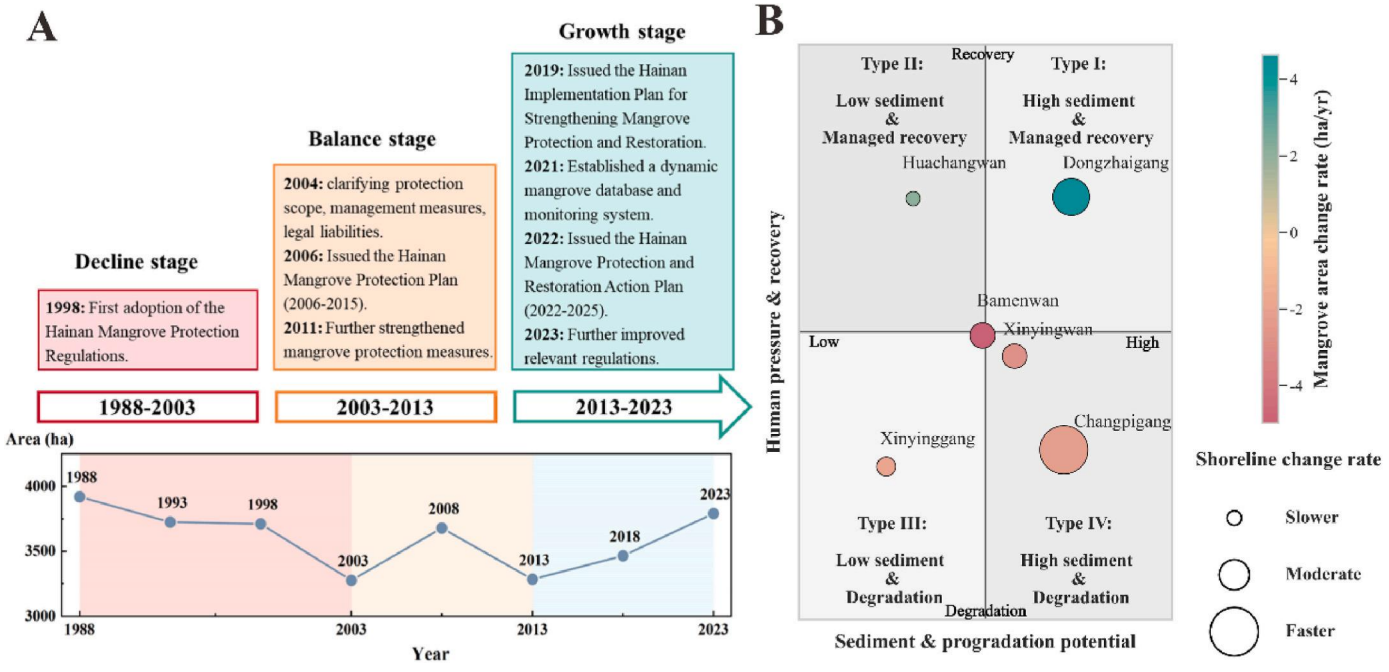

Fig. 10. Hainan's relevant policies and regulations on Mangrove Protection. (A) Stage-wise mangrove area evolution in Hainan Island in relation to major policy interventions, and (B) a two-dimensional classification of mangrove systems based on sediment and progradation potential and human pressure.

remain. The 30 m spatial resolution of Landsat imagery limits detection of small or fragmented mangrove patches, particularly newly planted seedlings (Hu et al., 2020). Although the spatial resolution of 30 m may limit the depiction of fragmented patches, the pixel size of 0.09 ha remains negligible relative to the total area of each reserve (Teluguntla et al., 2018). The long temporal consistency of Landsat data enables robust assessment of decadal trends, and classification accuracy remained high (Table S4). Additional uncertainties may arise from auxiliary datasets, including wave height, sea level, ocean current products, and TSM data, which may contain systematic biases related to spatial resolution, temporal sampling, or extreme events. They could influence interpretations of the impact of hydrodynamics on mangrove dynamics. Minor uncertainties may also arise from shoreline delineation. Boundaries in transitional zones or along mangrove edges may be ambiguous and digitization may introduce slight positional errors. Despite these limitations, the consistency of observed long-term patterns across multiple datasets supports the robustness of the conclusions. Future studies could further reduce uncertainty by integrating higher-resolution imagery and probabilistic accuracy assessments.

5. Conclusions

Mangrove forests on Hainan Island are mainly distributed along coastal lagoons and reef-fringed coasts. Based on mangrove dynamics from 1988 to 2023, this study shows that long-term mangrove trajectories are shaped by the interaction between governance measures and hydro-sedimentary processes in human-modified coastal systems. The main findings are.

1. From 1988 to 2023, Hainan's mangrove area declined overall by 129.25 ha. Mangrove dynamics followed three stages: early degradation (1988–2003), stabilization (2003–2013), and recovery (2013–2023). This three-phase trajectory illustrates a key governance principle: effective mangrove recovery requires the translation of legal protection into sustained management actions, providing a transferable governance pathway for restoring coastal wetlands under high anthropogenic pressure.
2. Early mangrove expansion occurred mainly on the landward side. After 2013, landward recovery combined with continued seaward advance offset previous losses, reversing the spatial pattern of mangrove decline. The mangrove shoreline advanced seaward at an average rate of 0.40 m/yr, with the most pronounced migration observed in Changpigang and Dongzhaigang. The expansion of seaward mangroves under rising sea levels occurs in sediment-rich, low-energy lagoon systems where sufficient sediment connectivity exists.
3. Early degradation resulted from large-scale aquaculture conversion, while recovery relied on the synergy of human interventions (pond-to-mangrove restoration, planting) and natural hydro-sedimentary processes. River- and tide-driven sediment transport promoted suitable substrates for expansion, whereas sea-level rise and wave action had a limited effect. Effective restoration thus requires aligning human actions with natural processes to sustain long-term resilience.
4. Long-term mangrove recovery requires spatially explicit strategies that account for local ecological conditions. Sediment-rich areas can expand naturally, while sediment-limited or altered sites need active restoration. Key strategies include: (1) protecting core forests, (2) converting ponds to mangroves while maintaining sediment connectivity and migration corridors, and (3) applying adaptive, near-natural governance to balance ecological integrity with sustainable coastal use. This integrated approach provides insights and policy guidance for mangrove restoration in tropical and subtropical regions.

CRediT authorship contribution statement

Bingnan Zhao: Writing – review & editing, Writing – original draft, Visualization, Methodology, Investigation, Formal analysis, Data curation. **Zhijun Dai:** Writing – review & editing, Writing – original draft, Project administration, Methodology, Investigation, Funding acquisition, Formal analysis, Data curation, Conceptualization. **Yuan Xiong:** Methodology, Investigation, Formal analysis, Data curation. **Chuqi Long:** Formal analysis, Data curation. **Xuefei Mei:** Investigation, Formal analysis, Data curation. **Jinping Cheng:** Methodology, Formal analysis, Data curation.

Declaration of competing interest

The authors declare that they have no known competing financial interests or personal relationships that could have appeared to influence the work reported in this paper.

Acknowledgements

This research was supported by the Shanghai International Science and Technology Cooperation Fund Project (23230713800, 23590780200; 24230740100), National Natural Science Key Foundation of China (NSFC) (41930537), and the Funds for Ministry of Science and Technology of China (SKLEC).

Appendix A. Supplementary data

Supplementary data to this article can be found online at https://doi.org/10.1016/j.jenvman.2026.129639.

Data availability

Data will be made available on request.

References

Adame, M.F., Neil, D., Wright, S.F., Lovelock, C.E., 2010. Sedimentation within and among mangrove forests along a gradient of geomorphological settings. Estuar. Coast Shelf Sci. 86 (1), 21–30. https://doi.org/10.1016/j.ecss.2009.10.013.

Amma, P.K.G., Bhaskaran, P.K., 2020. Role of mangroves in wind-wave climate modeling – a review. J. Coast Conserv. 24 (2), 21. https://doi.org/10.1007/s11852-020-00740-0.

Baig, M.R.I., Ahmad, I.A., Shahfahad, Tayyab, M., Rahman, A., 2020. Analysis of shoreline changes in vishakhapatnam coastal tract of Andhra Pradesh, India: an application of digital shoreline analysis system (DSAS). Annals of GIS 26 (4), 361–376. https://doi.org/10.1080/19475683.2020.1815839.

Belgiu, M., Drăguţ, L., 2016. Random forest in remote sensing: a review of applications and future directions. ISPRS J. Photogrammetry Remote Sens. 114, 24–31. https://doi.org/10.1016/j.isprsjprs.2016.01.011.

Blanton, A., Ewane, E.B., McTavish, F., Watt, M.S., Rogers, K., Daneil, R., et al., 2024. Ecotourism and mangrove conservation in southeast Asia: current trends and perspectives. J. Environ. Manag. 365, 121529. https://doi.org/10.1016/j.jenvman.2024.121529.

Breiman, L., 2001. Random forests. Mach. Learn. 45 (1), 5–32. https://doi.org/10.1023/A:1010933404324.

Bryan-Brown, D.N., Connolly, R.M., Richards, D.R., Adame, F., Friess, D.A., Brown, C.J., 2020. Global trends in mangrove forest fragmentation. Sci. Rep. 10 (1), 7117. https://doi.org/10.1038/s41598-020-63880-1.

Bunting, P., Rosenqvist, A., Hilarides, L., Lucas, R.M., Thomas, N., Tadono, T., Worthington, T.A., Spalding, M., Murray, N.J., Rebelo, L.-M., 2022. Global mangrove extent change 1996–2020: global mangrove watch version 3.0. Remote Sens. 14 (15), 3657. https://doi.org/10.3390/rs14153657.

Dai, Z., Long, C., Mei, X., Fagherazzi, S., Xiong, Y., 2024. Overestimation of mangroves deterioration from sea level rise in tropical deltas. Geophys. Res. Lett. 51 (19), e109675. https://doi.org/10.1029/2024GL109675.

Di Nitto, D., Neukermans, G., Koedam, N., Defever, H., Pattyn, F., Kairo, J.G., Dahdouh-Guebas, F., 2014. Mangroves facing climate change: landward migration potential in response to projected scenarios of sea level rise. Biogeosciences 11 (3), 857–871. https://doi.org/10.5194/bg-11-857-2014.

Diniz, C., Cortinhas, L., Nerino, G., Rodrigues, J., Sadeck, L., Adami, M., Souza-Filho, P. W.M., 2019. Brazilian mangrove status: three decades of satellite data analysis. Remote Sens. 11 (7), 808. https://doi.org/10.3390/rs11070808.

FAO, 2023. The World's Mangroves 2000–2020. https://doi.org/10.4060/cc7044en. Rome.

FAO, 2007. Food and agriculture organization of the united nations in the world's mangroves 1980–2005. Forest Resources Division, FAO. FAO Forestry Paper, Rome, p. 153.
Fenies, H., Faugères, J.-C., 1998. Facies and geometry of tidal channel-fill deposits (arcachon lagoon, SW France). Mar. Geol. 150 (1), 131–148. https://doi.org/10.1016/S0025-3227(98)00049-8.
Fu, G., Cao, C., Fu, K., Song, Y., Yuan, K., Wan, X., Zhu, Z., Wang, Z., Huang, Z., 2022b. Characteristics and evaluation of coastal erosion vulnerability of typical coast on Hainan Island. Front. Mar. Sci. 9, 1061769. https://doi.org/10.3389/fmars.2022.1061769.
Fu, C., Li, T., Cheng, K., Gao, Y., 2024. Inundation hazard assessment in a Chinese lagoon area under the influence of extreme storm surge. Water 16 (14), 1967. https://doi.org/10.3390/w16141967.
Fu, C., Song, X., Xie, Y., Wang, C., Luo, J., Fang, Y., Cao, B., Qiu, Z., 2022a. Research on the spatiotemporal evolution of mangrove forests in the Hainan island from 1991 to 2021 based on SVM and Res-UNet algorithms. Remote Sens. 14 (21), 5554. https://doi.org/10.3390/rs14215554.
Gan, H., He, H., Xia, Z., Li, F., 2018. Contamination assessment and source analysis for heavy metals and nutrient elements in sediments of the Yangpu Bay, Hainan Island. Earth Environ. 46 (5), 463–474 (in Chinese).
Gill, D.A., Mascia, M.B., Ahmadia, G.N., Glew, L., Lester, S.E., Barnes, M., et al., 2017. Capacity shortfalls hinder the performance of marine protected areas globally. Nature 543 (7647), 665–669. https://doi.org/10.1038/nature21708.
Giri, C., 2016. Observation and monitoring of mangrove forests using remote sensing: opportunities and challenges. Remote Sens. 8 (9), 783. https://doi.org/10.3390/rs8090783.
Giri, C., Ochieng, E., Tieszen, L.L., Zhu, Z., Singh, A., Loveland, T., Masek, J., Duke, N., 2011. Status and distribution of mangrove forests of the world using Earth observation satellite data. Global Ecol. Biogeogr. 20 (1), 154–159. https://doi.org/10.1111/j.1466-8238.2010.00584.x.
Goldberg, L., Lagomasino, D., Thomas, N., Fatoyinbo, T., 2020. Global declines in human-driven mangrove loss. Glob. Change Biol. 26 (10), 5844–5855. https://doi.org/10.1111/gcb.15275.
Hu, L., Xu, N., Liang, J., Li, Z., Chen, L., Zhao, F., 2020. Advancing the mapping of mangrove forests at national-scale using Sentinel-1 and Sentinel-2 time-series data with Google Earth Engine: a case study in China. Remote Sens. 12 (19), 3120. https://doi.org/10.3390/rs12193120.
Huete, A., Didan, K., Miura, T., Rodriguez, E.P., Gao, X., Ferreira, L.G., 2002. Overview of the radiometric and biophysical performance of the MODIS vegetation indices. Rem. Sens. Environ. 83 (1–2), 195–213. https://doi.org/10.1016/S0034-4257(02)00096-2.
Hamilton, S., 2013. Assessing the role of commercial aquaculture in displacing mangrove forest. Bull. Mar. Sci. 89 (2), 585–601. https://doi.org/10.5343/bms.2012.1069.
Harris, D.L., Rovere, A., Casella, E., Power, H., Canavesio, R., Collin, A., Pomeroy, A., Webster, J.M., Parravicini, V., 2018. Coral reef structural complexity provides important coastal protection from waves under rising sea levels. Sci. Adv. 4 (2), e4350. https://doi.org/10.1126/sciadv.aao4350.
Herbeck, L.S., Krumme, U., Andersen, T.J., Jennerjahn, T.C., 2020. Decadal trends in mangrove and pond aquaculture cover on Hainan (China) since 1966: mangrove loss, fragmentation and associated biogeochemical changes. Estuar. Coast Shelf Sci. 233, 106531. https://doi.org/10.1016/j.ecss.2019.106531.
Herbeck, L.S., Unger, D., Wu, Y., Jennerjahn, T.C., 2013. Effluent, nutrient and organic matter export from shrimp and fish ponds causing eutrophication in coastal and back-reef waters of NE Hainan, tropical China. Cont. Shelf Res. 57, 92–104. https://doi.org/10.1016/j.csr.2012.05.006.
Jiang, W., Huang, Z., Dai, Z., Luo, J., Zeng, W., Liang, X., 2025. Attenuation of hydro-sediment dynamics progradation over mangrove wetland. J. Geophys. Res., Oceans 130 (2), e021531. https://doi.org/10.1029/2024JC021531.
Kuenzer, C., Bluemel, A., Gebhardt, S., Quoc, T.V., Dech, S., 2011. Remote sensing of mangrove ecosystems: a review. Remote Sens. 3 (5), 878–928. https://doi.org/10.3390/rs3050878.
Le Nguyen, H.T., Luong, H.P.V., 2019. Erosion and deposition processes from field experiments of hydrodynamics in the coastal mangrove area of can Gio, Vietnam. Oceanologia 61 (2), 252–264. https://doi.org/10.1016/j.oceano.2018.11.004.
Li, R., Zhu, B., Tong, X., Yue, Y., Gan, H., Wan, S., 2017. Change analysis in Hainan dongzhai wetland reserve based on remote sensing data obtained during 2002-2013. Remote Sensing for Land & Resources 29 (3), 149–155 (in Chinese).
Li, Y., Wen, H., Wang, F., 2022. Analysis of the evolution of mangrove landscape patterns and their drivers in Hainan Island from 2000 to 2020. Sustainability 15 (1), 759. https://doi.org/10.3390/su15010759.
Liu, S., Huang, Y., Chen, H., Zhang, J., 2007. Vegetation index seasonal change and vegetation cover analyzing in Hainan Island. Res. Soil Water Conserv. 14 (2), 86–88 (in Chinese).
Liu, Y., Yu, R., Zheng, B., Liu, J., Song, Q., Chen, R., Yan, Z., 2022. Analysis of seasonal spatial and temporal variation patterns of forest vegetation NEP and climate drivers in Hainan Island. Journal of Tropical Biology 13 (2), 166–176. https://doi.org/10.15886/j.cnki.rdswxb.2022.02.008.
Long, C., Dai, Z., Wang, R., Lou, Y., Zhou, X., Li, S., Nie, Y., 2022. Dynamic changes in mangroves of the largest Delta in northern beibu gulf, China: reasons and causes. For. Ecol. Manag. 504, 119855. https://doi.org/10.1016/j.foreco.2021.119855.
Long, C., Dai, Z., Mei, X., Liang, X., Zhang, X., Xi, Y., Wang, R., Nguyen, B.A., Van, C.M., Cheng, J., 2025. Machine learning-based detection of dynamic changes in mangrove forest, beilun Estuary. Ocean Coast Manag. 266, 107696. https://doi.org/10.1016/j.ocecoaman.2025.107696.
Meng, Y., Gou, R., Bai, J., Moreno-Mateos, D., Davis, C.C., Wan, L., Song, S., Zhang, H., Zhu, X., Lin, G., 2022. Spatial patterns and driving factors of carbon stocks in mangrove forests on Hainan Island, China. Global Ecol. Biogeogr. 31 (9), 1692–1706. https://doi.org/10.1111/geb.13549.
Nassar, K., Mahmod, W.E., Fath, H., Masria, A., Nadaoka, K., Negm, A., 2019. Shoreline change detection using DSAS technique: case of North Sinai Coast, Egypt. Mar. Georesour. Geotechnol. 37 (1), 81–95. https://doi.org/10.1080/1064119X.2018.1448912.
Nevermann, H., AghaKouchak, A., Shokri, N., 2023. Sea level rise implications on future inland migration of coastal wetlands. Glob. Ecol. Conserv. 43, e02421. https://doi.org/10.1016/j.gecco.2023.e02421.
Nguyen, T.P., Luom, T.T., Parnell, K.E., 2017. Mangrove allocation for coastal protection and livelihood improvement in Kien Giang province, Vietnam: constraints and recommendations. Land Use Policy 63, 401–407. https://doi.org/10.1016/j.landusepol.2017.01.048.
Quang, D.N., Ngan, V.H., Tam, H.S., Viet, N.T., Tinh, N.X., Tanaka, H., 2021. Long-term shoreline evolution using DSAS technique: a case study of Quang Nam province, Vietnam. J. Mar. Sci. Eng. 9 (10), 1124. https://doi.org/10.3390/jmse9101124.
Rakotomavo, A., Fromard, F., 2010. Dynamics of mangrove forests in the mangoky River delta, Madagascar, under the influence of natural and human factors. For. Ecol. Manag. 259 (6), 1161–1169. https://doi.org/10.1016/j.foreco.2010.01.002.
Rouse Jr, J.W., Haas, R.H., Schell, J.A., Deering, D.W., 1973. Monitoring the vernal advancement and retrogradation (green wave effect) of natural vegetation. No. NASA-CR-132982) Available online: https://ntrs.nasa.gov/citations/19740022555.
Rodriguez-Galiano, V.F., Ghimire, B., Rogan, J., Chica-Olmo, M., Rigol-Sanchez, J.P., 2012. An assessment of the effectiveness of a random forest classifier for land-cover classification. ISPRS J. Photogrammetry Remote Sens. 67, 93–104. https://doi.org/10.1016/j.isprsjprs.2011.11.002.
Sandilyan, S., Kathiresan, K., 2012. Mangrove conservation: a global perspective. Biodivers. Conserv. 21, 3523–3542. https://doi.org/10.1007/s10531-012-0388-x.
Saintilan, N., Khan, N.S., Ashe, E., Kelleway, J.J., Rogers, K., Woodroffe, C.D., Horton, B. P., 2020. Thresholds of mangrove survival under rapid sea level rise. Science 368 (6495), 1118–1121. https://doi.org/10.1126/science.aba2656.
Seto, K.C., Fragkias, M., 2007. Mangrove conversion and aquaculture development in Vietnam: a remote sensing-based approach for evaluating the Ramsar convention on wetlands. Glob. Environ. Change 17 (3–4), 486–500. https://doi.org/10.1016/j.gloenvcha.2007.03.001.
Shi, T., Liu, J., Hu, Z., Liu, H., Wang, J., Wu, G., 2016. New spectral metrics for mangrove forest identification. Remote Sensing Letters 7 (9), 885–894. https://doi.org/10.1080/2150704X.2016.1195935.
Stone, G.W., Zhang, X., Sheremet, A., 2005. The role of barrier Islands, muddy shelf and reefs in mitigating the wave field along coastal Louisiana. J. Coast Res. 40–55. http://www.jstor.org/stable/25737048.
Taillie, P.J., Roman-Cuesta, R., Lagomasino, D., Cifuentes-Jara, M., Fatoyinbo, T., Ott, L. E., Poulter, B., 2020. Widespread mangrove damage resulting from the 2017 Atlantic mega hurricane season. Environ. Res. Lett. 15 (6), 064010. https://doi.org/10.1088/1748-9326/ab82cf.
Teluguntla, P., Thenkabail, P.S., Oliphant, A., Xiong, J., Gumma, M.K., Congalton, R.G., Yadav, K., Huete, A., 2018. A 30-m landsat-derived cropland extent product of Australia and China using random forest machine learning algorithm on Google Earth engine cloud computing platform. ISPRS J. Photogrammetry Remote Sens. 144, 325–340. https://doi.org/10.1016/j.isprsjprs.2018.07.017.
Thomas, N., Lucas, R., Bunting, P., Hardy, A., Rosenqvist, A., Simard, M., 2017. Distribution and drivers of global mangrove forest change, 1996–2010. PLoS One 12 (6), e0179302. https://doi.org/10.1371/journal.pone.0179302.
Thieler, E.R., Himmelstoss, E.A., Zichichi, J.L., Ergul, A., 2009. The digital Shoreline Analysis System (DSAS) version 4.0-an ArcGIS extension for calculating shoreline change. U.S. Geological Survey Open-File Report 2008-1278. http://doi.org/10.3133/ofr20081278.
Tian, P., Liu, Y., Li, J., Wang, H., Zhang, H., Ai, S., Ying, C., Zhong, J., 2024. Tracking annual changes of coastal aquaculture ponds in China during 1986–2021. Aquaculture 589, 740965. https://doi.org/10.1016/j.aquaculture.2024.740965.
Wang, L., Jia, M., Yin, D., Tian, J., 2019. A review of remote sensing for mangrove forests: 1956–2018. Rem. Sens. Environ. 231, 111223. https://doi.org/10.1016/j.rse.2019.111223.
Wu, R., Dai, Z., Mei, X., Luo, J., Fagherazzi, S., 2025. Profiling of mangrove forest dynamics in the Fly River delta, Papua New Guinea. Mar. Pollut. Bull. 217, 118119. https://doi.org/10.1016/j.marpolbul.2025.118119.
Xiao, X., Zhang, Q., Saleska, S., Hutyra, L., De Camargo, P., Wofsy, S., et al., 2005. Satellite-based modeling of gross primary production in a seasonally moist tropical evergreen forest. Rem. Sens. Environ. 94 (1), 105–122. https://doi.org/10.1016/j.rse.2004.08.015.
Xie, D., Schwarz, C., Kleinhans, M.G., Zhou, Z., van Maanen, B., 2022. Implications of coastal conditions and sea-level rise on mangrove vulnerability: a bio-morphodynamic modeling study. J. Geophys. Res.: Earth Surf. 127 (3), e06301. https://doi.org/10.1029/2021JF006301.
Xin, C.L., Ren, J.L., Zhang, G.L., Shao, Y.P., Zhang, G.L., Liu, S.M., 2013. Distributions and pollution status of heavy metals in the suspended particles of the estuaries and coastal area of eastern Hainan. Environmental Science 34 (4), 1315–1323 (in Chinese).
Xiong, Y., Dai, Z., Long, C., Liang, X., Lou, Y., Mei, X., Nguyen, B.A., Cheng, J., 2024. Machine Learning-Based examination of recent mangrove forest changes in the western Irrawaddy River Delta, Southeast Asia. Catena 234, 107601. https://doi.org/10.1016/j.catena.2023.107601.
Xu, H., 2006. Modification of normalised difference water index (NDWI) to enhance open water features in remotely sensed imagery. Int. J. Rem. Sens. 27 (14), 3025–3033. https://doi.org/10.1080/01431160600589179.

Yu, C., Liu, B., Deng, S., Li, Z., Liu, W., Ye, D., Hu, J., Peng, X., 2023. Using medium-resolution remote sensing satellite images to evaluate recent changes and future development trends of mangrove forests on Hainan Island, China. Forests 14 (11). https://doi.org/10.3390/f14112217. Article 11.

Yuan, R., Xu, R., Zhang, H., Hua, Y., Zhang, H., Zhong, X., Chen, S., 2024. Detecting shoreline changes on the beaches of Hainan Island (China) for the period 2013–2023 using multi-source data. Water 16 (7), 1034. https://doi.org/10.3390/w16071034.

Zeng, Y., Hao, D., Huete, A., Dechant, B., Berry, J., Chen, J.M., Joiner, J., Frankenberg, C., Bond-Lamberty, B., Ryu, Y., Xiao, J., Asrar, G.R., Chen, M., 2022. Optical vegetation indices for monitoring terrestrial ecosystems globally. Nat. Rev. Earth Environ. 3 (7), 477–493. https://doi.org/10.1038/s43017-022-00298-5.

Zhang, T., Hu, S., He, Y., You, S., Yang, X., Gan, Y., Liu, A., 2021. A fine-scale mangrove map of China derived from 2-meter resolution satellite observations and field data. ISPRS Int. J. GeoInf. 10 (2), 92. https://doi.org/10.3390/ijgi10020092.

Zhang, L., Tang, Y., Lin, J., Yan, M., Liao, J., 2022. A Dataset of Aquaculture Ponds in Hainan Island Based on Landsat Data During 1987–2020, 2022. Science Data Bank. https://doi.org/10.11922/sciencedb.j00001.00400, 2022-12-19.

Zhou, G., Cao, X., Xia, J., Song, Z., 2024. Holocene sedimentary geochemical characteristics of the mid-eastern part of the Beibu Gulf and their implications. Geochimica 53 (5), 745–759 (in Chinese).

Zhu, B., Liao, J., Shen, G., 2021. Spatio-temporal simulation of mangrove forests under different scenarios: a case study of mangrove protected areas, Hainan Island, China. Remote Sens. 13 (20), 4059. https://doi.org/10.3390/rs13204059.